Available online at www.sciencedirect.com
SCIENCE DIRECT®
PERGAMON
Acta Astronautica 56 (2005) 65–71
ACTA ASTRONAUTICA
www.elsevier.com/locate/actaastro

Detection and analysis of high-temperature events in the BIRD mission

Boris Zhukov*, Klaus Briess, Eckehard Lorenz, Dieter Oertel, Wolfgang Skrbek

DLR, Institute of Space Sensor Technology and Planetary Exploration, Rutherfordstr. 2, 12489 Berlin, Germany

Available online 22 October 2004

Abstract

The primary mission objective of a new small Bi-spectral InfraRed Detection (BIRD) satellite is detection and quantitative analysis of high-temperature events like fires and volcanoes. An absence of saturation in the BIRD infrared channels makes it possible to improve false alarm rejection as well as to retrieve quantitative characteristics of hot targets, including their effective fire temperature, area and the radiative energy release. Examples are given of detection and analysis of wild and coal seam fires, of volcanic activity as well as of oil fires in Iraq. The smallest fires detected by BIRD, which were verified on ground, had an area of 12 m^2 at daytime and 4 m^2 at night.

1. BIRD Mission

The primary mission objective of a new small Bi-spectral InfraRed Detection (BIRD) satellite, which was put in a 570 km circular Sun-synchronous orbit on 22 October 2001, is detection and quantitative analysis of high-temperature events (HTE) like fires and volcanoes [1]. The principal BIRD imaging payload includes the Hotspot Recognition System (HSRS) with channels in the Mid-Infrared (MIR: 3.4– 4.2 μm) and Thermal Infrared (TIR: 8.5–9.3 μm) spectral ranges and the Wide-Angle Optoelectronic Stereo Scanner (WAOSS-B) with a nadir channel in Near-Infrared (NIR: 0.84–0.90 μm) spectral range. Two other off-nadir stereo channels of WAOSS-B are currently not used for hotspot detection. The ground resolution of the BIRD nadir channels is 185 m in the NIR and 370 m in the MIR and TIR. However, all three channels have the same sampling step of 185 m due to an oversampling by a factor of 2 of the MIR and TIR data.

A unique feature of the BIRD MIR and TIR channels is a real-time adjustment of their integration time [2]. If onboard processing of HSRS data indicates that detector elements are saturated, or close to saturation in the first exposure, then a second exposure is performed within the same sampling interval with a reduced integration time. The data of both exposures are merged on ground. This eliminates detector saturation over high-temperature targets but preserves a 0.1–0.2 K radiometric resolution for pixels at normal temperatures [3].

* Corresponding author.
E-mail address: boris.zhukov@dlr.de (B. Zhukov).

0094-5765/$ - see front matter © 2004 Elsevier Ltd. All rights reserved.
doi:10.1016/j.actaastro.2004.09.014

Due to the better resolution of the HSRS channels, BIRD can detect hot targets with a factor of 7 smaller area than MODIS and AVHRR. The oversampling of the BIRD MIR and TIR data enhances the re-sampling accuracy during data co-registration and reduces the effect of fire detectivity deterioration at pixel edges. Potentially, it allows also a resolution enhancement.

2. Hotspot detection and analysis algorithm

The BIRD hotspot detection and analysis algorithm [4] includes the following principal tests:

(a) adaptive MIR radiance thresholding to detect potential hot pixels: $I_{\mathrm{MIR}} \geqslant k I_{\mathrm{MIR,bg}}$,
(b) NIR reflectance thresholding to reject strong Sun glints and clouds (only at daytime): $\rho'_{\mathrm{NIR}} \leqslant 0.6$,
(c) adaptive MIR/NIR radiance ratio thresholding to reject high-reflective objects (only at daytime): $I_{\mathrm{MIR}}/I'_{\mathrm{NIR}} \geqslant k I_{\mathrm{MIR,bg}}/I_{\mathrm{NIR,bg}}$,
(d) adaptive MIR/TIR radiance ratio thresholding to reject warm surfaces: $I_{\mathrm{MIR}}/I'_{\mathrm{TIR}} \geqslant k I_{\mathrm{MIR,bg}}/I_{\mathrm{TIR,bg}}$,
(e) pixel contrast test to reject impulse noise,
(f) consolidation of hot pixels in hot clusters (hotspots).

Since fires have the largest contrast with the background in the MIR spectral range (Fig. 1), the MIR thresholding is applied as the first test to select potential hot pixels. The following tests (b–e) are used to reject false alarms.

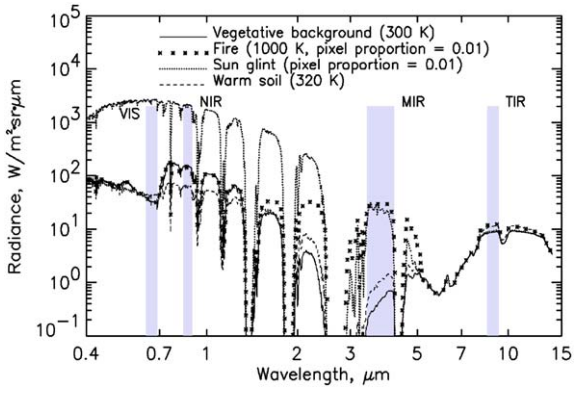

Fig. 1. Spectral radiance of a fire at the top of the atmosphere in comparison to the spectral radiance of vegetative background, Sun glints and warm soils (simulations).

Sun glints, which may have as high MIR radiance as fires with the same pixel proportion (Fig. 1), are rejected using the MIR/NIR radiance ratio (here we have to use the NIR radiance instead of the VIS radiance that would be optimal for this purpose). Before the MIR/NIR thresholding, a thresholding of the NIR reflectance is applied to reject strong Sun glints and clouds that may saturate the BIRD NIR channel and thus distort the MIR/NIR test.

Warm surfaces that occupy a whole pixel may have a similar MIR radiance as small fires (Fig. 1). They are rejected using the MIR/TIR radiance ratio.

The thresholds in the adaptive tests (a), (c) and (d) are made proportional to the corresponding characteristics of the background that are calculated using the median background radiances in the NIR, MIR and TIR channels $I_{\mathrm{NIR,bg}}$, $I_{\mathrm{MIR,bg}}$ and $I_{\mathrm{TIR,bg}}$. In order to account for regional and temporal background variations, the background characteristics are defined separately for each 1000 image lines, corresponding to on-ground areas of $\sim 200 \times 200$ km. For global investigations, the factor k can be selected to be equal to 2.2 at daytime and to 1.6 at night, providing a reliable rejection of false alarms in a wide range of observation conditions. For investigations at specific sites, lower values of coefficient k may be sufficient, allowing detection of smaller hotspots. However, it requires 'teaching' the algorithm for each specific site.

With the aim to relax the effect of inter-channel co-registration errors, we use in the hotspot detection tests (b–d) the maximal values I'_{NIR} and I'_{TIR} of the NIR and TIR radiances in a 3×3 window around a potential hot pixel.

In order to distinguish actual hot pixels from impulse noise, which occurred in ~3% of the BIRD data dumps, a pixel contrast test (e) was introduced. It checks if the contrast of a potential hot pixel in the MIR is consistent with the Point Spread Function (PSF) of the BIRD MIR channel.

The consolidation of hot pixels in hot clusters (f) is performed by a simple clustering procedure that assigns adjacent hot pixels to the same cluster.

The following characteristics are computed for each hot cluster (hotspot):

- centre co-ordinates,

- effective fire temperature T_F and effective fire area A_F,
- radiative fire energy release (FRE).

Furthermore, the front length and the front strength (FRE per 1 m of the fire front) are estimated for pronounced fire fronts in the BIRD data.

The effective fire temperature and area are the temperature and area of a homogeneous fire at a uniform background that would produce the same MIR and TIR radiances as the actual non-homogeneous fire. T_F and A_F can be retrieved with the bi-spectral technique [5] that solves the fire-background mixing equations in the MIR and TIR channels using an estimation of the background radiance from the neighbouring pixels. In contrast to the usual application of the bi-spectral technique, we apply it not to separate hot pixels but to entire hot clusters, thus reducing the effect of MIR/TIR inter-channel co-registration errors and of MIR/TIR PSF difference.

Since the TIR channel is relatively low sensitive to small fires, the TIR background variability can lead to errors of a few hundred Kelvin in the retrieved fire temperature unless the fire proportion in a hotspot exceeds 0.25–1% of the cluster area [4,6]. We estimated the effect of the background errors by varying the background components in the mixing equations in the range of ± 1 standard deviation of the background radiance [4].

Additional offsets in the estimated hotspot parameters are possible due to sensor calibration errors and errors in accounting for the atmospheric effects and for fire emissivity. Their effect on the bi-spectral retrievals is usually significantly smaller than the effect of the TIR background error, except for large fires.

Many hotspots in the BIRD data have a low fire proportion making the fire temperature and area estimation for them unreliable. A possibility to improve the retrieval accuracy for these parameters at night by using additional NIR data is discussed in Section 3.

The FRE is a more stable parameter for a quantitative characterisation of both large and small fires [7,8] and therefore it is principally used for coding hotspots in the standard BIRD data products. The FRE is useful for parameterisation of the amount of burning fuel, as well as for practical fire fighting purposes where the energy release per unit length of a fire front characterises the front strength. We use two methods of radiative energy release estimation: (a) FRE calculation based on the effective fire temperature and area as retrieved by the Bi-spectral technique and (b) the MIR radiance method [8] that is based on a regression of FRE with the MIR radiance that is valid only for fire temperatures above 600–700 K .

3. Examples of hotspot detection and quantitative analysis

During nearly 2 years of its operation, BIRD has detected numerous vegetation, peat and coal seam fires, volcanic events and industrial hotspots worldwide. Some examples of the recent BIRD results are given below.

Fig. 2 illustrates the BIRD potential for fire detection in the daytime and at night. The hotspot in the white circle in a daytime BIRD image in Fig. 2a was verified to correspond to a small fire with an area of 12 m^2 ($\sim 10^{-4}$ of the pixel area of the BIRD IR channels). Fig. 2b shows a small controlled wood fire with an area of only 4 m^2 (3×10^{-5} of the IR pixel area) arranged at night during a BIRD overflight. The bi-spectral and MIR radiance methods gave a close estimation of its FRE of 0.11–0.14 MW. It is in a reasonable agreement with onground fire temperature measurements of 930–990 K that would result in emission of 0.17–0.22 MW from 4 m^2 (one should take into account that this value may be overestimated since the peripheral fire parts could have a lower temperature).

Fig. 3 shows an image of large forest fires in the south-east of Australia, which was obtained by BIRD on 26 January 2003 in the MIR spectral channel, and the detected hot clusters that are coded with their estimated FRE values. Fires were already extinguished in the immediate vicinity of the capital Canberra but intensive burning was still going on to the south-west of it. Two large fire clusters in the lower part of the image radiate 50 and 170 GW of thermal energy, which is ~80% of the total radiative FRE in the scene (280 GW). These are the most intensive fires detected until now by BIRD. The effective fire temperature T_F of these fires was $\sim$ 1000 K, indicating intensive flaming burning. The T_F values for other fires in the scene ranged typically from 600 to 1000 K, but for many of the smaller fires these retrievals were unreliable.

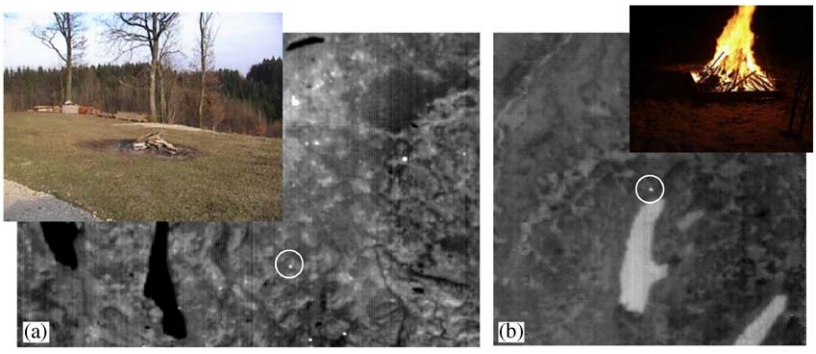

Fig. 2. Verification of the BIRD hotspot detection: (a) fire with an area of 12 m^2 detected at daytime; (b) controlled fire with an area of 4 m^2 detected in the night.

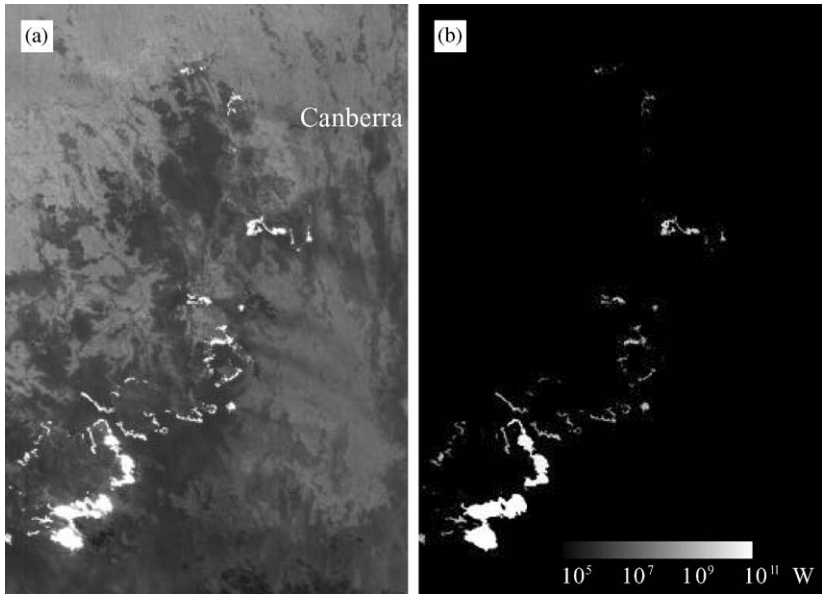

Fig. 3. Forest fires in the area of Canberra, Australia imaged by BIRD on 26 January 2003: (a) MIR band; (b) detected hot clusters and their radiative energy release.

From end of January 2002 until January 2004, BIRD monitors coal seam fires in the Ningxia and Xinjiang areas of China. Fig. 4 shows an example of coal seam fire detection in the day- and night time BIRD images of the Rujigou coalfield that was verified by an on-ground inspection in September 2002. The daytime MIR image (Fig. 4a) shows a few hotspots that allow detection and estimation of their energy release (Fig. 4c). They can be associated with stronger coal seam fires (and in one case with an industrial chimney) mapped on ground within a few days of the BIRD data take. However, some of the weaker fires could not be detected at daytime due to the masking effect of the reflected solar radiation and of background temperature variations. The night time BIRD MIR image data (Fig. 4b)— in spite of a moderate signal-to-noise ratio—allowed recognition of most of the weaker coal fires and an estimation of their FRE (Fig. 4d). The

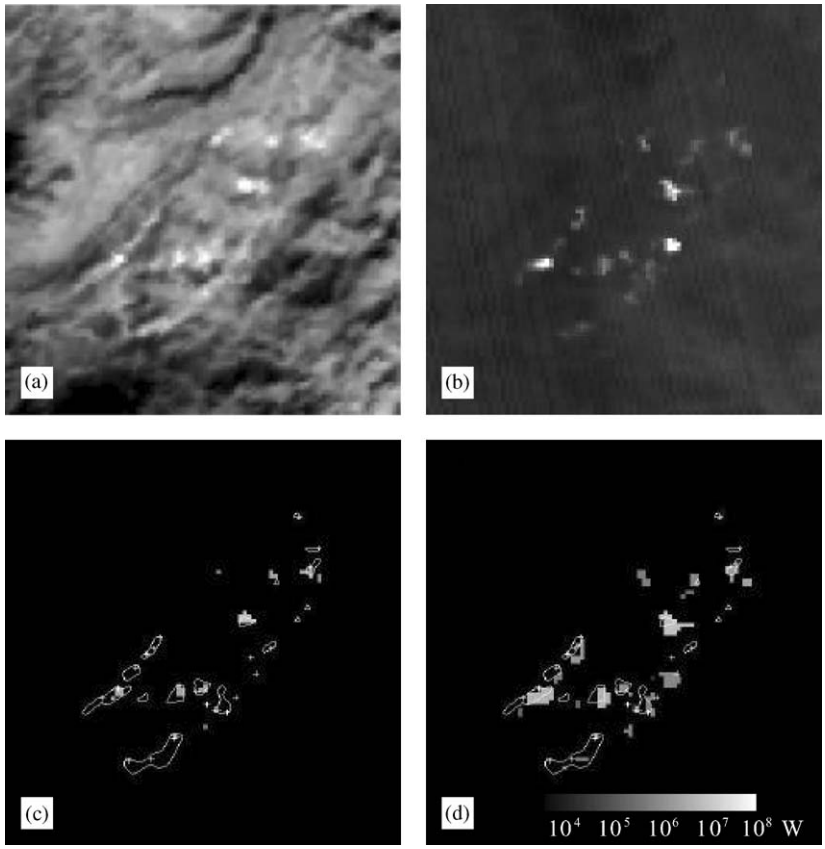

Fig. 4. Coal fire detectiion in the BIRD images and comparison with ground truth: (a) daytime MIR image obtained on 21 September 2002; (b) night time MIR image obtained on 16 January 2003; (c) radiative energy release of detected hotspots at daytime; (d) radiative energy release of detected hotpots at night; white contours and crosses indicate location of coal seam fires verified on ground in September 2002, while white triangles show location of industrial chimney.

effective temperature of most of the fires was in the range of 300–400 K, which is significantly lower than typical coal burning temperatures. It indicates that the radiation of the warm surface around the fires dominates in the signal of the detected hotspots. The radiative energy release of the coal seam fires ranges from $\sim$ 0.01 MW for the weakest detected (at night time) fires up to $\sim$10 MW for the strongest fires.

As an example of volcanic activity detection by BIRD, Fig. 5 shows hotspots at Etna and Stromboli volcanoes detected on 2 November 2002 during their reported eruptions. A lava flow from the northern crater of Etna is characterised by $T_F = 540$ K, $A_F = 25$ Ha and FRE = 1.1 GW. Three other hotspots at Etna emitted between 30 and 160 MW of radiative power. Warm older lava as well as a strong

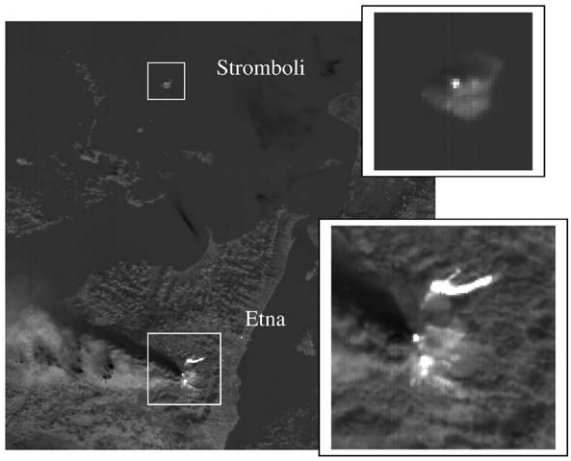

Fig. 5. Hotspots at Etna and Stromboli in the BIRD MIR image of 2 November 2002.

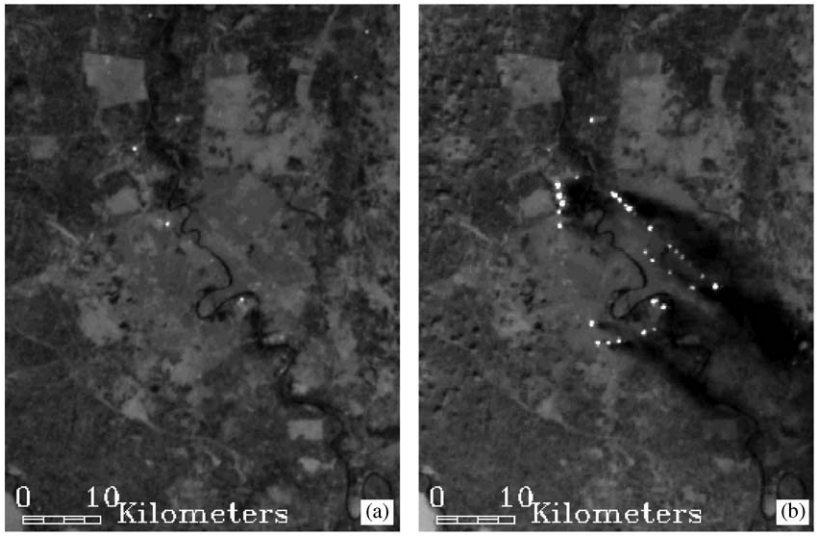

Fig. 6. Hotspots in daytime MIR images of Baghdad obtained by BIRD before and during the war: (a) 13 March 2003; (b) 27 March 2003.

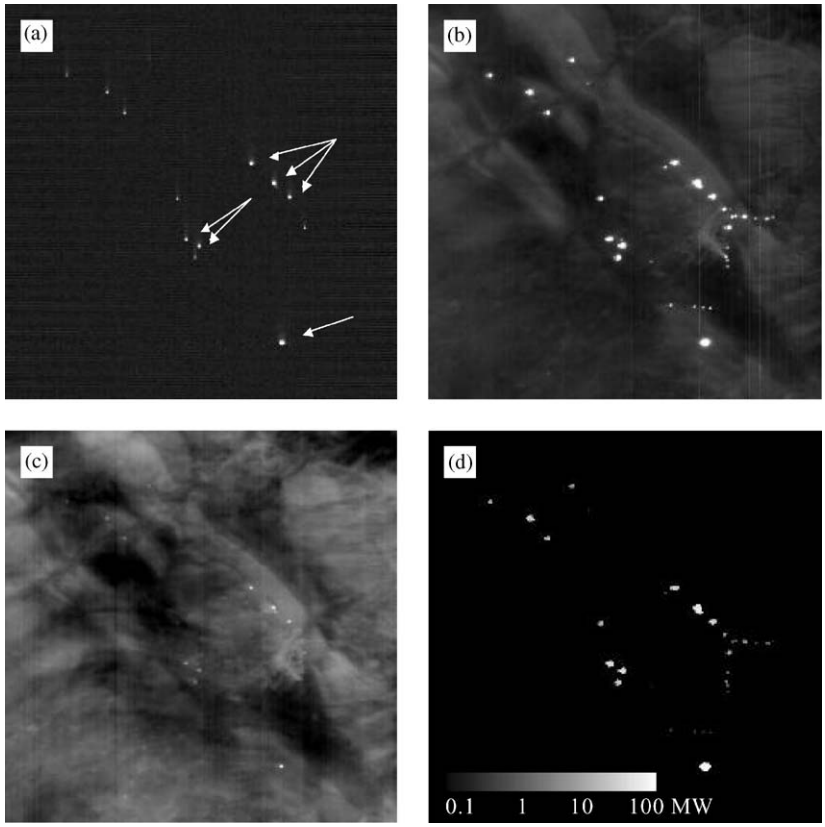

Fig. 7. BIRD night time detection of oil fires in the area of Kirkuk, Iraq on 4 April 2003: (a) NIR image; (b) MIR image; (c) TIR image; (d) detected hotspots coded with their FRE; arrows mark hotspots with a strong NIR signal, for which an accurate estimation of the effective fire temperature and area is possible.

smoke plume were the other prominent features of the Etna image fragment. The activity of Stromboli was lower—the detected hotspot emitted only 4 MW.

Fig. 6 compares MIR images of Baghdad obtained by BIRD on 13 March 2003 (before the war) and on 27 March 2003 (during the war). On 13 March 2003, a few hotspots can be recognised that have probably an industrial origin (in particular, the hotspot in the south of Baghdad corresponds to the oil refinery). During the war, numerous additional hotspots appeared in the scene, most of which evidently correspond to burning oil trenches. Dark smoke originating from the fires is also clearly seen. The energy release of the fires ranged from 0.3 to 50 MW.

In the night, conditions for hotspot detection and analysis are more favourable than in the daytime. Lower background radiance in the MIR and TIR channels allows detection of smaller fires, while lower background radiance variability allows a more accurate retrieval of fire characteristics. Additionally, the NIR channel can also register signal of high-temperature fires, making possible a more accurate estimation of their characteristics.

As an example, Fig. 7 shows night time NIR, MIR and TIR images of oil fires in the area of Kirkuk during the Iraq war. Thirty-one hotspots are prominent in the MIR image (Fig. 7b). Some of them are clearly seen also in the NIR image (Fig. 7a). These hotspots can be identified also in the TIR image (Fig. 7c), but their contrast there is significantly lower than in the NIR. Utilising the NIR channel in addition to the MIR and TIR channels for the fire temperature and area retrieval made it possible to improve significantly the retrieval accuracy. Six hotspots with the strongest NIR signal, which are marked in Fig. 7a with arrows, allow a rather accurate estimation of the effective fire temperature and area. For them, relatively high effective temperatures are retrieved ranging from 1500 to 1750 K. The standard deviation of the retrieved temperature, which was defined by varying the background values in all three channels, did not exceed 20 K. The effective fire area for them ranged from 60 to 370 m^2. In case when only the MIR and TIR channels were used for the retrievals, the error intervals were very large, with the lower bound ranging from 650 to 850 K and the upper bound being uncertain.

In the other cases, when the NIR signal of the hotspots was week or they could not be recognised in the NIR at all, the error range for the effective fire temperature was usually covering practically all the possible fire temperature range.

4. Conclusion

BIRD has demonstrated its potential for detection and quantitatively evaluation of high-temperature events like vegetation-, oil- and coal seam fires and volcanic activity. It allows estimation of the radiative fire energy release and—for larger fires—their effective temperature and area. In the night, utilisation of the NIR data in addition to the MIR and TIR data makes it possible to improve significantly the fire temperature and area retrieval accuracy for very hot targets like oil fires.

References

[1] K. Briess, H. Jahn, E. Lorenz, D. Oertel, W. Skrbek, B. Zhukov, Remote sensing potential of the Bi-spectral InfraRed Detection (BIRD) Satellite, Int. J. Remote Sens. 24 (2003) 865–872.
[2] W. Skrbek, E. Lorenz, HSRS—An infrared sensor for hot spot detection, Proc. SPIE 3437 (1998) 167–176.
[3] E. Lorenz, W. Skrbek, Calibration of a bi-spectral infrared push-broom imager, Proc. SPIE 4486 (2001) 90–103.
[4] B. Zhukov, K. Briess, E. Lorenz, D. Oertel, W. Skrbek, BIRD Detection and Analysis of High-temperature Events: First Results, Proc. SPIE 4886 (2003) 160–171.
[5] J. Dozier, A method for satellite identification of surface temperature fields of subpixel resolution, Remote Sens. Environ. 11 (1981) 221–229.
[6] L. Giglio, J.D. Kendall, Application of the Dozier retrieval to wildfire characterization—a sensitivity analysis, Remote Sens. Environ. 77 (2001) 34–49.
[7] Y.J. Kaufman, C.O. Justice, L.P. Flynn, et al., Potential global fire monitoring from EOS-MODIS, J. Geophys. Res. 103 (1998) 32215–32238.
[8] M. Wooster, B. Zhukov, D. Oertel, Fire radiative energy release for quantitative study of biomass burning: derivation from the BIRD experimental satellite and comparison to MODIS fire products, Remote Sens. Environ. 86 (2003) 83–107.